Resonant bond wire vibrations in the ATLAS semiconductor tracker

T.J. Barber[a], D.G. Charlton[b], M. Warren[c], W. Murray[d], G. Villani[d], A.R. Weidberg[e],*

[a]*Physics Department, Cambridge University, UK*
[b]*School of Physics and Astronomy, The University of Birmingham, UK*
[c]*Department of Physics and Astronomy, University College London, UK*
[d]*Rutherford Appleton Laboratory, UK*
[e]*Physics Department, Denys Wilkinson Building, Oxford University, Keble Road, Oxford, OX13RH, UK*

Abstract

Dangerous mechanical resonances exist which can lead to the breaking of bond wires if time varying currents are passed through them in a magnetic field. The results of analytic calculations and an FEA analysis are described. The results of experimental investigations using wire bonds on test circuits are given. The possible effects within the ATLAS SCT were investigated and a fixed frequency trigger veto algorithm, designed to minimise the dangers of breaking wire bonds, was developed.
© 2004 Elsevier B.V. All rights reserved.

1. Introduction

In the presence of a magnetic field, B, a wire of length l, carrying a current, I, will experience a

Lorentz force, $F = BIl$. For typical bond wires of length 2 mm carrying currents of 10 mA in a magnetic field of 2 T, the magnitude of this force is 4×10^{-5} N, which is more than three orders of magnitude smaller than the minimum force required to break a wire bond, which is of the order of 0.1 N. Therefore, even relatively large DC currents do not represent any significant danger. However, if the current is varying with time at a

*Corresponding author. Tel.: +44 1865 273370; fax: +44 1865 273417.
E-mail address: t.weidberg1@physics.ox.ac.uk (A.R. Weidberg).

frequency close to one of the mechanical resonance frequencies of a bond wire, then a strong resonant vibration will start, which will usually lead to the failure of the bond wire after a period of a few seconds to minutes. Such effects were seen by the CDF collaboration in the SVXII detector and several detector modules failed because of the resulting broken wire bonds [1]. CDF implemented administrative measures to avoid any dangerous fixed frequency running conditions and have not subsequently seen any more such problems [2].

Optical links will be used in the ATLAS SemiConductor Tracker (SCT) and Pixel detector [3,4] to transmit data from the detector modules to the off-detector electronics and to distribute the Timing, Trigger and Control (TTC) data from the counting room to the front-end electronics [5]. The currents from the VCSEL Driver Chip (VDC) to the on-detector VCSELs form 25 ns long pulses when a data "1" is being transmitted. Therefore, there will be a burst of current during the transmission of event data after receipt of a level 1 (L1) trigger. There is, therefore a potential danger of resonant wire bond vibrations if L1 s are issued at a fixed frequency close to a resonant frequency.

In Section 2 a general theoretical analysis of resonant wire bond vibrations is presented. The results of analytic calculations are summarised and the results of more detailed FEA calculations are described. Experimental measurements of resonant wire bond vibrations for test wire bonds are given in Section 3. The results of searches for resonances with test structures with wire bonds identical to those that will be used in ATLAS are also presented in Section 3. In order to minimise the danger due to resonant wire bond vibrations an algorithm was developed to veto dangerous fixed frequency triggers and this is discussed in Section 4. Finally some conclusions are drawn in Section 5.

2. Calculations of resonant bond wire vibrations

The results of simple analytic calculations are given in Section 2.1 and the results of more detailed FEA calculations are given in Section 2.2.

2.1. Analytic calculations

In a simple analytical model of a bond wire, consider a straight beam of material, length l, diameter d, which is clamped at both ends. If the wire were constrained to oscillate in only one dimension, it would be expected that the first two normal modes of oscillation would have the form shown in Fig. 1. For a higher frequency mode, n, there would be $n-1$ nodes, but the shapes would be similar.

To find the shape and frequencies of the oscillations, we can consider the wire as a loaded beam [6]. It can be shown that the resonant frequency of the first normal mode is

$$\omega = \frac{kd}{l^2} \qquad (1)$$

where k is a constant depending on the properties of the wire and the amplitude of the oscillation a, scales with the length of the bond wire as

$$a = cl^4 \qquad (2)$$

where c is another constant depending on the properties of the wire.

2.2. FEA calculations

A number of bond wires were constructed using the JL Analyser FEA package [7]. The parameters used for constructing these models were the bond length, diameter and the loop height. A simple quadratic curve was fitted to these variables to give

Fig. 1. Shape of the first two normal modes.

an estimation of the bond shape, with a 0.1 mm foot length at either end. The model was then meshed as a circular beam and given the following properties consistent with wire bonds for ATLAS:

Young's modulus	69 GPa
Density	2710 kg m^{-3}
Poisson's ratio	0.330

A side view of the bond model is shown in Fig. 2.

To mimic attachment to the bond pad, restrictions in all degrees of freedom were imposed on both of the bond feet. Frequency analysis was performed on a number of bonds to find the frequencies of the normal modes. The shapes of the first four modes are shown in Fig. 3.

The shapes of the odd numbered modes are those predicted using the analytic beam model earlier (compare with Fig. 1). The even numbered modes correspond to displacements in the plane of the wire. As there will be Lorentz forces in both directions due to the different orientations of bond wires in the ATLAS magnetic field, both types will be considered.

A plot of the normal mode frequencies versus bond wire length is shown in Fig. 4 and the expected variation of resonant frequency with length from the analytic calculations ($f \propto 1/l^2$)

Fig. 4. Plot of FEA calculations of the inverse square of the resonant frequency versus bond wire length for different modes. The straight lines shown are fits for modes 1 and 3.
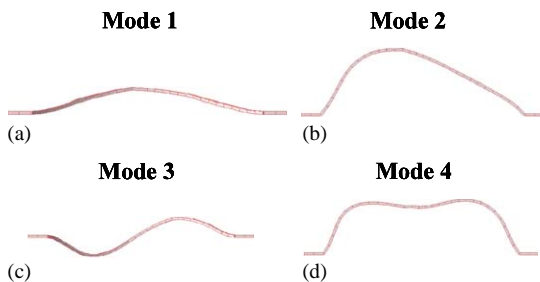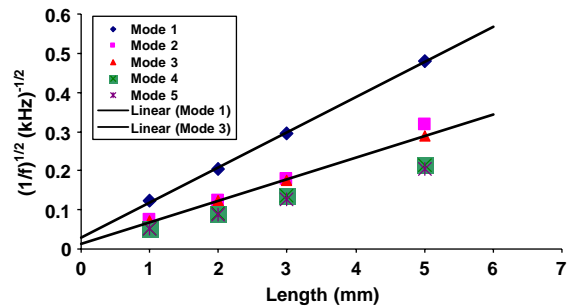
Fig. 2. FEA model for a bond wire.

Fig. 3. Shapes of the first four normal modes. With the wire bond in the vertical plane, modes 1 and 3 are shown looking from above and modes 2 and 4 are shown from the side.

of Section 2.1 is seen apart from a small offset. The FEA calculations also showed that the normal mode frequencies have a direct proportionality with bond diameter as expected from the analytic calculations. The FEA calculations also predicted some variation of the resonant frequency with bond loop height. For a range of bond heights between 0.2 and 0.3 mm the expected change in resonant frequency was ~9%.

Some FEA calculations were also carried out with ANSYS, a more advanced FEA package, using a more realistic bond wire, with $l = 2.6$ mm and $h = 1.4$ mm. This showed the same shapes of normal modes as before, with a fundamental frequency at 13.5 kHz. A spectrum analysis could also be performed using a sinusoidal Lorentz driving force of 5.2×10^{-5} N.[1] The forces were applied in both the Y (in the plane of the bond wire loop) and Z (perpendicular to the plane of the bond wire loop) directions to simulate the possible orientations in the magnetic field in ATLAS. The responses are shown in Figs. 5 and 6.

These show that the Y & Z direction forces will excite the even and odd numbered modes, respectively. The plots show that the Y direction amplitude is roughly two orders of magnitude smaller than that for the Z. In the Y direction case the amplitude is an order of magnitude less than the diameter of a bond wire, so will probably not be a problem in ATLAS. The fundamental of the

---

[1]Calculated from a 20 mA current, 2 T field and 2.6 mm of wire, using $F = BIl$.
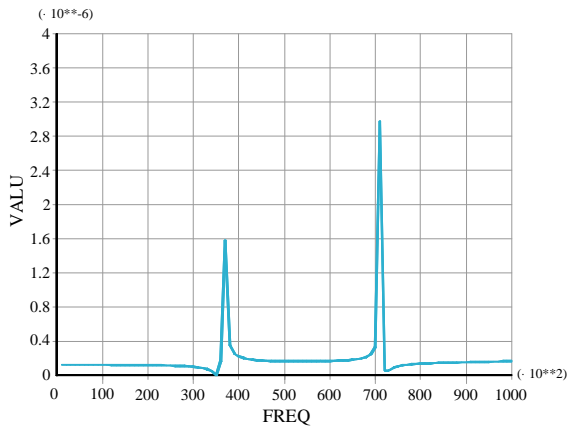
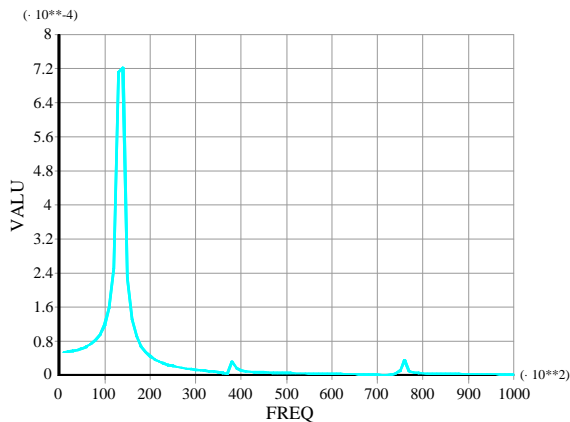Fig. 5. Frequency response in the Y direction.

Fig. 6. Frequency response in the Z direction.

Z direction response shows a much larger magnitude and should be easy to detect and would be expected to lead to bond wire breaking if the resonance was excited.

2.3. Summary of calculations

The main conclusions from the analytic and FEA calculations are that the resonant frequency depends on the length of the bond wire as $f \propto 1/l^2$ and the amplitude scales as $a \propto l^4$. Therefore, shorter bond wires will have very high-resonant frequencies with very small amplitudes whereas longer bond wires will have lower resonant

frequencies and much larger amplitude oscillations.

3. Experimental study of resonant bond wire vibrations

The first very simple tests were carried out using a video camera to image test wire bonds placed inside the Birmingham superconducting magnet facility. The magnetic field was limited to 0.5 T, to avoid degradation of the image quality by the stray magnetic field, but the amplitude of the current oscillation was increased to 40 mA to compensate. The test wire bonds were made with the same length as those used in the ATLAS SCT barrel opto-package to connect the VDC ASIC to the VCSELs. The magnetic field was in the plane of the loop of the bond wire, i.e. perpendicular to that which will be used in ATLAS. The frequency of the current through the bonds was scanned in the range 10–100 kHz and strong resonances were visible at a frequency around 15 kHz. When the set-up was left running on resonance, the wire bonds were observed to fail suddenly after a few minutes. This showed that there was a potential problem with resonant wire bond breaking in ATLAS.

More detailed studies were carried out at the Rutherford Appleton Laboratory using a 1.8 T dipole magnetic field. Two different techniques were used to study the wire bond vibrations:

1. The wire bonds were viewed directly with a CCD camera equipped with a high-magnification lens. The images were read out at an adjustable frequency as the frequency of the current through the wire bond was scanned. Since the resonance frequencies were much higher than the inverse of the time per frame, any vibrations of the wire bond would lead to the image of the wire bond being fuzzy. A very crude estimate of the amplitude of the vibration could be obtained from the width of the fuzzy image of the wire bond.
2. The presence of a vibrating wire bond in the magnetic field leads to a back e.m.f. across the wire bond. A step pulse was applied to the wire

bond with an amplitude of 1 V and a duration of 1ms. The voltage across the wire bond was monitored with an oscilloscope to look at the resulting free oscillations at the end of the pulse. The signals were averaged over a large number (1000–4000) of sweeps to reduce the effects of noise. A Fast Fourier Transform (FFT) was performed by the oscilloscope. A resonant wire bond vibration would produce a peak in the resulting FFT spectrum.

The results with test wire bonds are discussed in Section 3.1 and the search for resonant wire bond vibrations with ATLAS SCT components are presented in Section 3.3.

3.1. Test wire bonds

The first set of experiments uses test bond wires to help classify the general nature of the oscillations and resonant frequencies. Short bond wires (lengths less than 1 mm) were used initially and as expected no resonances large enough to be seen with the video camera were observed. Clear evidence for resonant vibrations was obtained using the back e.m.f. method. The response of the system with and without the field is shown in Fig. 7, averaged over 1000 sweeps. The response

shown is from bond wire number 4 on the test board.

With the field on there appears to be a high-frequency oscillation superimposed onto a lower frequency signal ($\sim$1 kHz). This low frequency is unlikely to be from bond wire oscillations, but could be due to other components of the board reacting to the magnetic field. The most likely candidates are the wires used to connect the signal cable to the actual bonds. From the simulations, a signal in the 1 kHz range could be caused by a 5 cm length of copper wire, comparable to the lengths of actual wires used. The higher frequency signal is likely to be a bond wire oscillating. An FFT of the two signals is shown in Fig. 8.

There is a clear peak in the FFT, which does not appear with the field switched off. The peak also shifts from positive to negative at its highest point, implying a phase change across this region. The peak occurs at 89.5 ± 0.5 kHz which is consistent with a bond wire with a length of 0.85 mm and a loop height of 0.3 mm.

To investigate this further, the wire above and three others were tested in the field but this time averaged over 4000 sweeps to decrease errors. Four wires were tested and their frequencies are shown in Table 1. In two cases the negative side of the peak was not seen; this may be because the
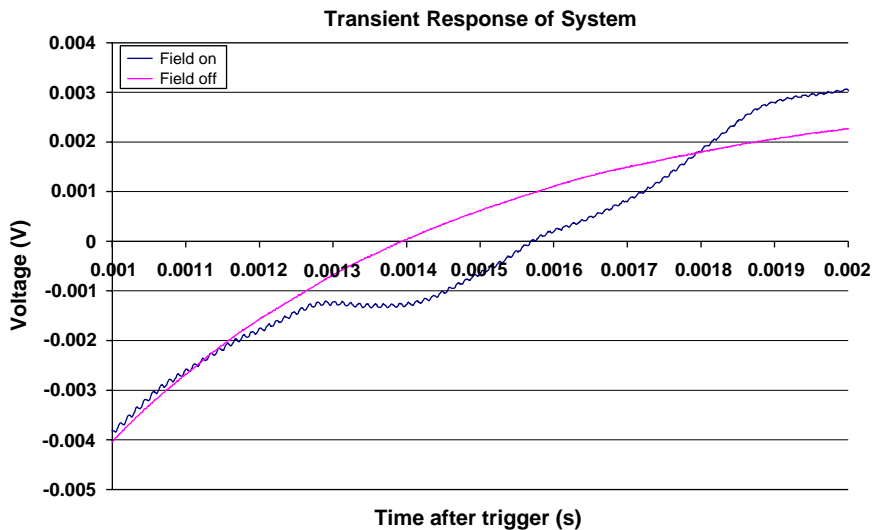

Fig. 7. Response measured on a short bond wire to a transient pulse with the magnetic field on and off.
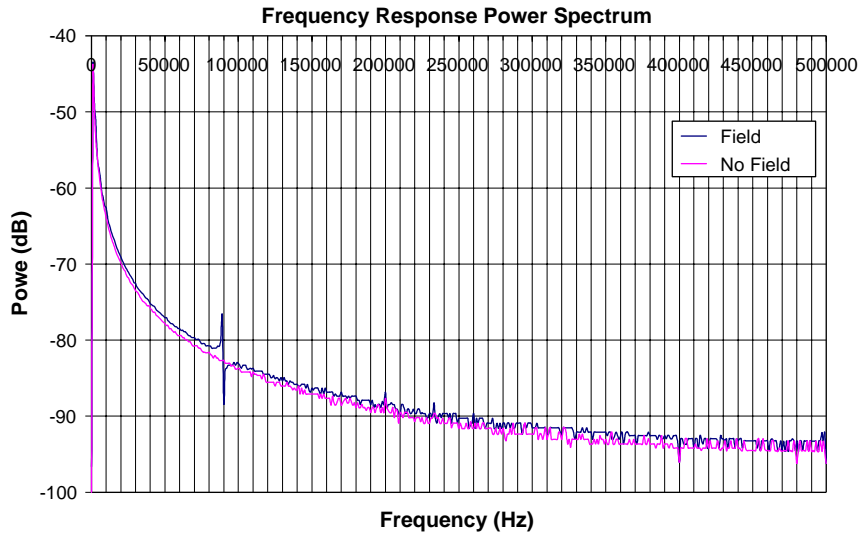
Fig. 8. FFT spectrum of back emf signal from a short bond wire (with and without magnetic field).

Table 1
Resonant frequencies for short bond wires

Bond wire number	Frequency (kHz)	Amplitude (dB)
3	74	5.1
4	90	5.8
5	75	2.7
6	69	12.2
Mean	77	6.5
Std. Dev	9	4.0

resonance is too narrow for the FFT resolution so only the positive peak is displayed. There was a significant variation in amplitudes of the peaks compared to the surrounding level. This could be partly explained by the fact that these resonances are very narrow compared to the experimental resolution. Visual inspection of the wires after the experiment revealed that the smaller amplitude wire had been distorted, which also could be partly the cause.

The standard deviation corresponds to a frequency variation of ∼12%, giving a length variation of 6%. Assuming all of this error comes from the placement of two bond feet at each end of the wire, the accuracy of the bonding machine would be ∼27 μm.

An FFT of the voltage with no bond wire, (i.e. a shorted track) showed no peak in the spectrum, but still contained the low-frequency resonance, demonstrating that it is not a bond wire effect. Also, changing the orientation in the field to give a force in the plane of the wire loop showed no peak. This is expected, as a different set of modes are excited by this orientation of field with much lower amplitudes (see Section 2.3). It would therefore, be expected that the peaks moved and would be too small to be detected.

Longer bonds were also tested to try and obtain visual confirmation of the resonance. The lengths of the bond wires were 2.3 mm. To study the sensitivity to the wire bonding quality, three of the wire bonds were deliberately "over-bonded". This was achieved by applying too much power or pressure. The other four bond wires were bonded in the standard way to produce the normal bond heel. The back e.m.f. method was used to locate the approximate position of the resonant frequencies before trying to view them directly. As expected, these bonds show lower resonant frequencies with much larger amplitudes, due to their length. An example of the back e.m.f. FFT for one of the bonds is shown in Fig. 9.

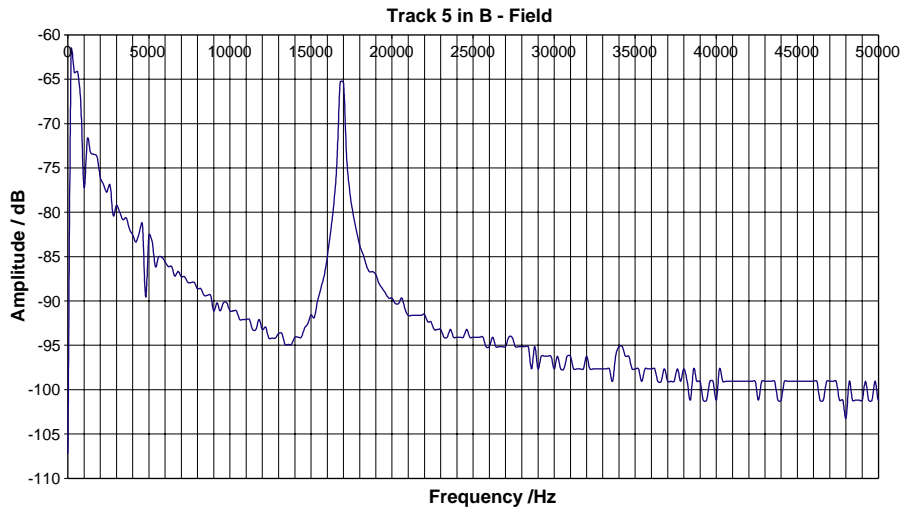The resonance is now much clearer at 17.0 ± 0.2 kHz and there is a hint of a first

Fig. 9. FFT of back e.m.f. signal for a long wire bond.

Table 2
Resonant frequencies for long bond wires

Bond wire number	Frequency (kHz)
5	17.0
6	17.8
7	18.6
8	18.0
Mean	17.9
Std. Dev	0.7

harmonic at 34.6 ± 0.2 kHz. The resonant frequencies of four wires were measured using this method and are summarised in Table 2.

The FEA prediction for a bond wire of 2.3 mm and a 0.3 mm loop height is 18.0 kHz, and so is in very good agreement. Once again, the mean and standard deviation correspond to a bond foot placement error of about 25 μm

The bond wire number 7 was scanned with a constant current sine wave of 10 mA from 15 to 20 kHz and the wire width appeared to increase as it reached resonance. Closer to the resonant frequency the wire is clearly oscillating, as the extremes of movement appear bright with a dark area between. The largest amplitude of oscillations occurred at 17.4 kHz, which is significantly lower than predicted by the back e.m.f. method. This

may be because the system is not linear and the current used for the back e.m.f. method was larger than that used for the constant current sine wave. Photos of the oscillating bonds are shown in Figs. 10 and 11.

When trying to scan other bonds with sinusoidal currents, the resonance seemed to disappear. After showing a clear peak with the e.m.f. method and initial oscillations close to resonance, a scan over the frequencies showed no difference in width. Returning to the e.m.f. method revealed the peak had disappeared. This happened with the three remaining bonds and the cause is still unknown. It is possible that initial fatigue due to driving at resonance or close to it for a short time may prevent oscillations from reoccurring until a recovery time has elapsed.

The wires may have warmed making them more malleable or cracks may have prevented oscillation. However, the earlier tests performed at the superconducting magnet facility at Birmingham showed that bond wires that were excited at the resonant frequency were likely to break after a few minutes of operation. Therefore these results therefore confirm the dangers of wire bonds breaking due to resonant bond wire vibrations reported in Ref. [1], although they show that sometimes a resonant vibration may start and then stop without the wire bond breaking.

Fig. 10. Photo of a wire bond with a current of frequency 15 kHz, away from resonance.

Fig. 11. photograph of a wire bond with a current of frequency 17 kHz, on resonance.

3.2. Q factor of resonances

The quality factor of an oscillation (Q factor) is defined by

$$Q = \omega \frac{\langle U \rangle}{\langle P \rangle} \tag{3}$$

where ω is the angular frequency, $\langle U \rangle$ is the average energy stored per cycle, $\langle P \rangle$ is the average power dissipated per cycle. The Q factor for the resonances of the 2.3 mm bonds can be evaluated by three different methods.

3.2.1. Transient response

The transient responses of bond wire numbers 3 (over-bonded) and 5 (normal bond) as measured using the back e.m.f. method were fitted to a series

of three decaying sinusoidal oscillations (corresponding to damped SHM solutions) of the form

$$A = A_0 \exp(-\gamma_0 t) \sin(\omega_0 t + \phi_0) \\ + A_1 \exp(-\gamma_1 t) \sin(\omega_1 t + \phi_1) + \dots . \tag{4}$$

A plot of the fit is shown in Fig. 12.

The fit shows some low-frequency components at around 1 kHz, probably due to other wires in the system, and a higher frequency component at around 17 kHz, due to the bond wire. The Q value in this case can be derived as follows:

$$Q = \frac{\omega_0}{2\gamma}. \tag{5}$$

A summary of the high-frequency components' properties is shown in Table 3. Both of the frequencies agree with the previous measurements from the FFT peaks within experimental error.
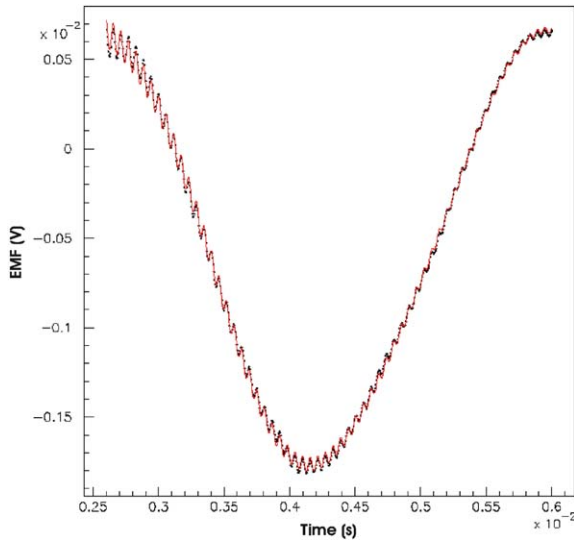
Fig. 12. Back emf signal with sinusoidal fit of the form of Eq. (4) superimposed.

Table 3
Summary of fit values

Bond wire number	Frequency (kHz)	$\gamma/(2\pi)$ (Hz)	Quality factor
3	16.9 ± 1.6	46.6 ± 4.4	181 ± 24
5	17.3 ± 0.4	77.2 ± 1.9	112 ± 4

3.2.2. Width of power spectrum

The Q factor can also be given by

$$Q = \frac{\omega_0}{\Delta\omega} \tag{6}$$

where ω_0 is the resonant frequency and $\Delta\omega$ is the full-width half-maximum (FWHM) of the peak in the power spectrum. This can be evaluated from the FFT curves obtained from the back e.m.f. method. A summary of the results is shown in Table 4.

3.2.3. Amplitude versus frequency fitting

Analysis of the photographs of bond wire number 7 at frequencies close to resonance gives an estimate of the actual amplitude of the oscillating wires. The square of this amplitude gives a value proportional to the power spectrum

Table 4
Summary of fit values. The error on all frequency measurements is ± 50 Hz. The first 3 bond wire numbers correspond to "over-bonded" wire bonds and the last 4 bond wire numbers correspond to standard wire bonds

Bond wire number	Frequency f_0 (kHz)	Bandwidth Δf (Hz)	Q factor
1	17.37	250	69 ± 14
2	13.81	200	69 ± 17
3	17.30	340	51 ± 7
		Mean:	57
		Std. dev	13
5	16.90	320	53 ± 8
6	17.76	270	66 ± 12
7	18.60	150	124 ± 41
8	17.99	190	95 ± 25
		Mean	75
		Std. dev	33

of oscillations that can be fitted to the Lorentzian peak predicted from driven SHM solutions:

$$p = \frac{(\gamma^2/4)H}{(\omega - \omega_0)^2 + (\gamma^2/4)} \tag{7}$$

where H is the peak height, ω_0 the resonant frequency, γ the FWHM of the peak. The best fit gives values of $f_0 = 17.4$ kHz, $\Delta f = 100$ Hz and so $Q = 172 \pm 43$. This is in agreement with the FFT method in the previous section for bond wire number 7. The plot of the data points and the fitted curve are shown in Fig. 13 and indicate a good fit at frequencies close to the resonance, but seems to underestimate the data far from the resonance. This may indicate that there may be other factors in the system not accounted for by the Lorentzian.

In conclusion, the quality factor of the oscillations has been measured using three different techniques and broadly similar results have been obtained. At this precision there seems to be no difference between over-bonded and normal wires.

3.3. Wire bonds in ATLAS SCT components

Having investigated the phenomenon of bond wire resonance in test bond wires, more specific
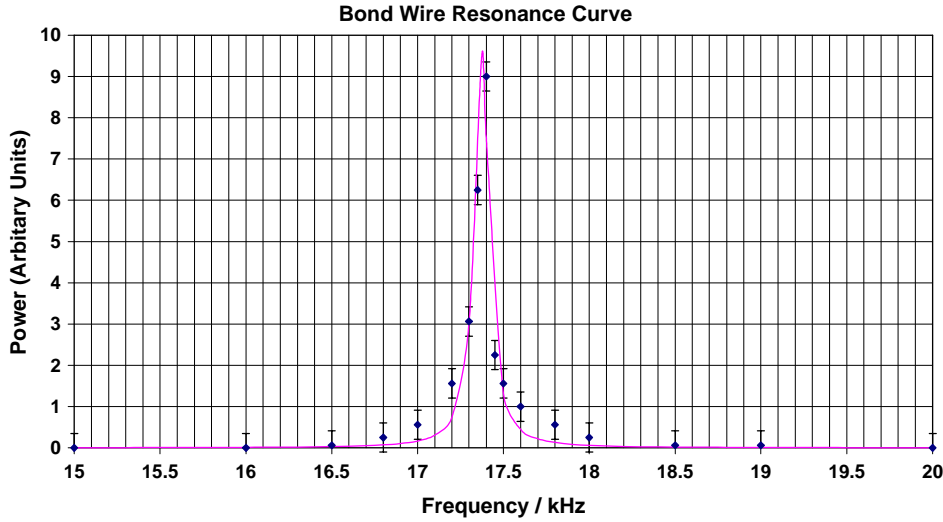
Fig. 13. Power versus frequency for a wire bond resonance. The superimposed curve is a fit to Eq. (7).

Table 5
Conditions for wire bonds to be liable to undergo resonant vibrations

Parameter or condition	Value
Current change on receipt of L1 trigger	$> \sim 1\,mA$
Orientation of bond wire with respect to solenoidal magnetic field.	$\sim 90°$

tests were done on pieces of ATLAS hardware that could be at risk from resonance. The conditions for wire bonds to be vulnerable to resonant wire bond vibrations in ATLAS operation are listed in Table 5.

The wire bonds in the SCT that satisfy these conditions are those that carry current from the VDC [8] to the VCSELs [9] in the opto-packages [10,11]. In the barrel opto package (mounted on a Cu/kapton flex circuit) the magnetic field will be perpendicular to the wire loop ("barrel" mode), so will excite the even modes as in Section 2.2, which are likely to have very small amplitude. The forward opto packages (mounted onto the forward SCT hybrids) have bonds with the magnetic field in the plane of the wire loop, so excite the more dangerous odd modes ("forward" mode).

3.3.1. Barrel opto-package

The bonds that carry analogue output signals from the VDC chip to the VCSELs on the barrel opto packages were monitored with the camera and scanned over a frequency range from 16 to 20 kHz with a 10 mA square wave, to simulate a worst case ATLAS scenario. Both the "forward" and "barrel" orientations of field were tested although in ATLAS only the "barrel" case will occur. As the current through the bonds is controlled by the VDC ASIC it was not possible to monitor the voltage across them directly and so the back e.m.f. method could not be used.

In "forward" mode two sets of resonant frequencies were found for each wire, a fundamental frequency, f, and a resonance at $f/3$. The lower frequency square wave will contain a Fourier component at the fundamental and hence should excite it with lower amplitude. The fundamental frequencies of the two wires were 17.2 and 18.0 kHz (± 0.1 kHz). This is slightly higher than that expected from the FEA calculations, which predicted a fundamental frequency in the range 13.2 to 14.0 kHz corresponding to the length range of 2.74–2.65 mm with a loop height of 0.3 mm. The loop height variation may be responsible for this discrepancy.
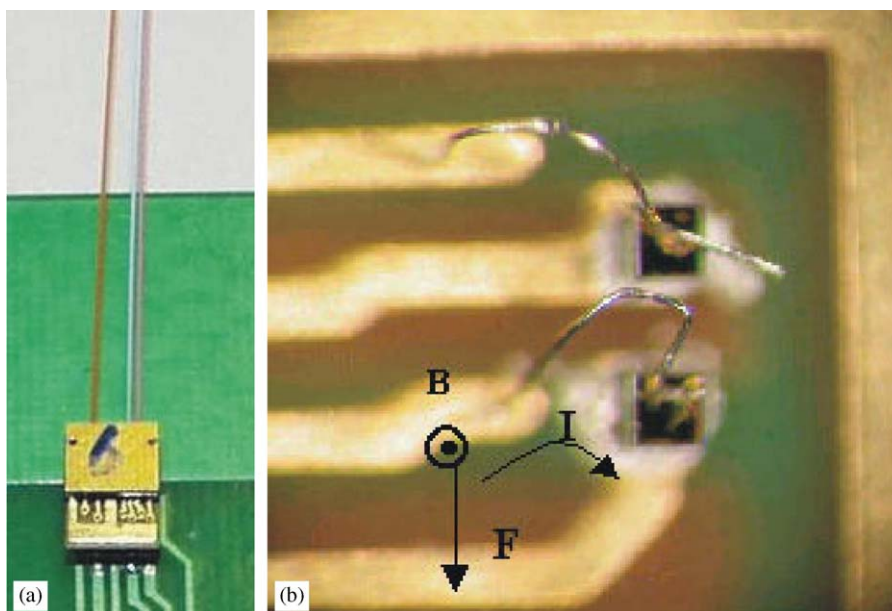
Fig. 14. Forward opto plug-in. (a) Package with 3 pig-tailed fibres, (b) close-up of wire bonds from PCB tracks to VCSELs.

In "barrel" mode no resonance could be seen up to 50 kHz despite a predicted resonant frequency between 33 and 36 kHz. An oscillation with a displacement of one bond wire width would have been detected, therefore the amplitude of any resonance must be smaller than 25 μm.

3.3.2. Forward opto-package

The two bond wires to the VCSEL chips are in the "forward" orientation but are fairly short (less than 1 mm) so are expected to have high-frequency, low-amplitude oscillations. The wires were driven directly through a resistor to give 25 mA. Only 10 mA is expected in normal ATLAS operating conditions (Fig. 14).

The back e.m.f. method showed no peaks up to a frequency of 500 kHz. This puts an upper limit on resonant peaks at 4 μV compared to the 80 μV peak for the 2.3 mm long bond wires. Visual scans up to 150 kHz revealed no oscillations with amplitude greater than about $\frac{1}{4}$ of a bond wire diameter.[2] Four wires were tested in total.

The wires are estimated to be 0.67 mm long with a 0.21 mm loop height. Predictions from FEA calculations give an extrapolated fundamental at 131 ± 11 kHz. This is encouraging, as there are unlikely to be triggers sent at above 100 kHz so that any resonances above this will only be hit with higher frequency, lower amplitude Fourier components. This, combined with the low-amplitude resonance, indicates that these bonds are unlikely to be at risk.

3.3.3. Forward hybrid

Similar methods were used to investigate the bond wires for the VDC ASIC on the forward SCT hybrid [12]. Two pairs of bond wires carry digital data in LVDS [3] format from the hybrid to the ASIC. The AC component of the LVDS signal in each bond wire is 4 mA. The back e.m.f. method

---

[2] When looking for "barrel" mode oscillations the bond wires were imaged directly by the CCD camera, whereas in

(*footnote continued*)
"forward" mode the bond wires were viewed through a mirror, which degraded the resolution of the image. Therefore, a smaller amplitude resonance would be detectable in "barrel" mode (Section 3.3.1) than in "forward" mode (Section 3.3.2).

[3] Low Voltage Differential Signals(LVDS) for Scalable Coherent Interface (SCI) Draft 1.3. IEEE P1596.3-1995.

was used to search for resonances in these bond wires and a scan revealed no resonances with amplitudes larger than $4\,\mu V$ up to $500\,kHz$. Visual scans with the CCD camera were made of four different bond wires carrying the output current from the VDC to the hybrid and also showed no resonance in the region between 50 and $150\,kHz$. A square wave current was used to pulse the wires.

The predicted resonant fundamental frequency for bond wires with a length of $0.7\,mm$ is $118 \pm 10\,kHz$. Their short length also means that a small amplitude would be expected, around 100 times smaller than the $2.3\,mm$ long test bonds, due to the fourth power relationship. As the largest amplitude seen with the long wires was ~ 16 wire diameters, the largest corresponding amplitude for the forward SCT hybrid bonds is less than 0.2 diameters. As the bond wire showed up as 4 pixels wide on the CCD image, it is not surprising nothing was seen. On this scale it would be very hard to locate the exact resonant frequencies to test the bond wire durability. Prolonged exposure to low-amplitude resonant pulses may still, however, be enough to break the bonds by metal fatigue.

4. Trigger veto algorithms

As a result of the combination of the favourable orientation with respect to the magnetic field (barrel opto-package) and short bond wires (forward opto-package and ASICs) the amplitudes of any resonant vibrations in the SCT will be very small. Although they would not be expected to lead to any immediate failures, metal fatigue is still a concern for longer term operation. Since the production of the components is well advanced the option of adding a potting compound at the feet of the wire bonds to damp the oscillations is not a practical option. A large additional safety factor can be obtained if one can avoid any fixed frequency trigger operation as explained in Section 4.1. A proposed algorithm to veto fixed frequency trigger operation is described in Section 4.2.

4.1. Frequency spectrum of random triggers

In normal ATLAS data taking, physics triggers will occur at random times so that the frequency spectrum associated with currents in the read-out circuitry will be very broad. A very simple Monte Carlo simulation of the time structure of the readout was used to calculate this frequency spectrum. L1 triggers were generated at an average frequency of $75\,kHz$ (the maximum trigger rate expected in ATLAS). The current pulse associated with the resulting readout was generated from a uniform distribution between 0 and $10\,\mu s$, although it was checked that the frequency spectrum was very insensitive to the nature of this distribution. The resulting frequency spectrum is very wide and the fraction of the power contained in any narrow resonance is very small. For example, for a resonance at a frequency of $17\,kHz$ and a width of $124\,Hz$ (the average of the measurements for long bond wires described in Section 3.2) the power contained within the width of the resonance is only 0.3% of the total. Therefore, the danger due to resonant wire bond vibrations from physics triggers is greatly reduced compared to operation with a fixed frequency clock operating at a wire bond resonant frequency.

4.2. Proposed trigger veto algorithm

Although fixed frequency running will not occur in normal Physics operation in ATLAS, there is a danger that it will occur in special runs during development and tests of the trigger system. Therefore a fixed frequency trigger veto algorithm will be implemented in the SCT TIM module [13] to avoid this danger. The algorithm is based on the one being implemented by the CDF collaboration; if there are more than N triggers with a difference in time between successive triggers of less than ΔT, a veto is generated. A development of this simple algorithm has been implemented to consider only fixed frequencies that are above some cut, f_{cut}. The suggested starting values [14] are $N = 10$ and $= \Delta T$ $1\,\mu s$. The value of f_{cut} was set to $15\,kHz$. This would, therefore allow for single bunch operation of the LHC during the machine start-up [15] but provide full protection against any dangerous
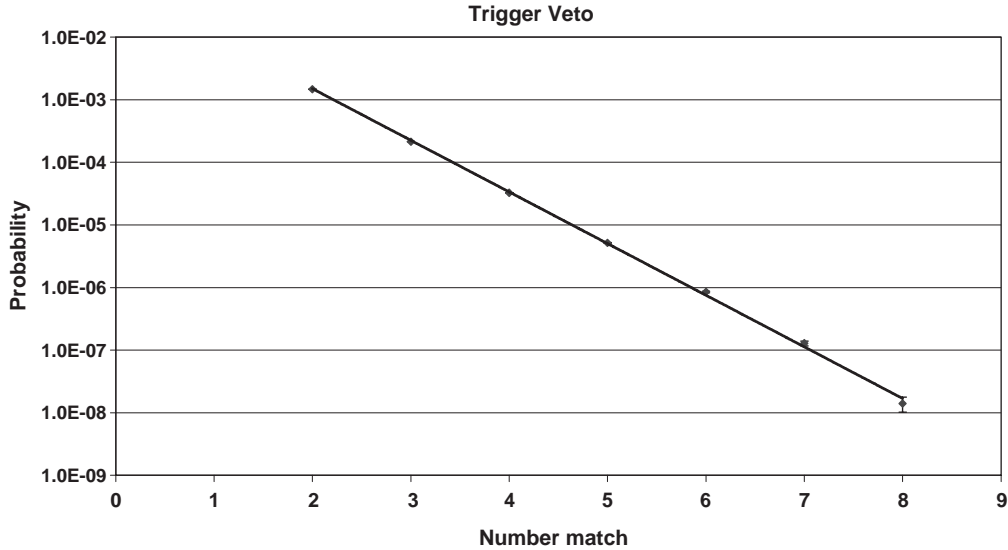
Trigger Veto

Fig. 15. Probability of the fixed frequency trigger veto algorithm wrongly vetoing a genuine random trigger as a function of the number of matching trigger time differences required to create a veto. The superimposed line is a result of an exponential fit.

frequencies close to the resonances in the wire bonds. A simple "toy" Monte Carlo programme was used to estimate the probability of generating a trigger veto with this algorithm, assuming that the triggers were generated randomly in time (with an exponential distribution in time between successive triggers). The results of this calculation are shown in Fig. 15. For the default values ($N = 10$ and $= \Delta T$ 1 µs) and the worst-case L1 trigger rate of 75 kHz, the predicted veto probability for a random trigger is $\sim 4 \times 10^{-10}$. If further triggers are vetoed for a period of 1 ms after the trigger veto algorithm detects an apparent fixed frequency trigger, the resulting dead time fraction will be $\sim 3 \times 10^{-8}$. Therefore this type of simple algorithm can be used to veto efficiently a fixed frequency trigger whilst generating a negligible dead time for genuine physics triggers.

4.2.1. Implementation in TIM

A TIM is located in each SCT Read-Out Driver (ROD) crate, where it interfaces and fans-out triggers from the Timing, Trigger and Control (TTC) to the RODs via the crate backplane. It also aggregates the busy signals from each ROD card, and transfers this back to the TTC system. This is,

therefore, an ideal place to locate an SCT sub-detector specific fixed frequency trigger veto (FFTV) system.

As the TIM design is in its final pre-production phase, the FFTV is required to fit into the existing architecture. The TIM's main functions are implemented in programmable logic chips (FPGA's) and, as such, it has no on-board processing. To avoid a large-scale redesign, it is desirable that the FFTV be built using spare logic resources inside an existing FPGA chip. To ensure the system could be integrated easily, it was felt that the focus should be on keeping it as small as possible.

4.2.2. Fixed frequency detection

Fourier analysis would provide the optimal separation between fixed frequency and random triggers. Fast Fourier Transforms (FFTs) are widely used in programmable-logic designs. Early trials were with a user-customisable FFT 'core' supplied ready-made with Xilinx firmware development software.[4] Testing the design showed it to
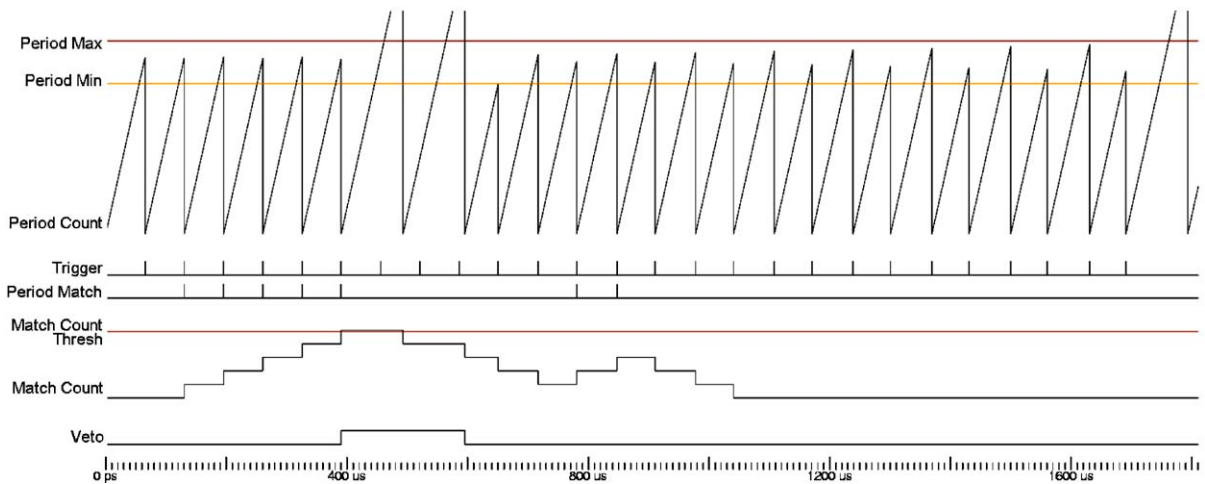
---
[4]http://www.xilinx.com/ipcenter/catalog/logicore/docs/vfft32.pdf.

Fig. 16. Demonstrates the veto generated after 5 successive triggers, as well as trigger matching some nonidentical low ΔT trigger periods. Note that during a veto the period counter continues counting beyond the scope of this plot.

be resource hungry—using over 50% of a large FPGA—and over specified for the application. To keep resource utilisation to a minimum, focus was shifted toward a more application specific algorithm. Therefore, the simpler algorithm described in Section 4.2 was implemented in the FPGA.

4.2.3. Repetitive period monitoring

To detect fixed frequencies it is easier to think in terms of repetitive intervals between successive triggers, and work with these values on an FPGA. By counting clocks between each trigger and storing the results, successive trigger periods are checked for equality (i.e. a match). Each time there is a match, a match counter is incremented, with transgression of a pre-defined limit generating a veto. If there is no match, the match counter is decremented.

In the cases where triggers stop, the period counter continues to a user-defined maximum and rolls over to zero. Each time it rolls over the match-counter is decremented. This sets the decay rate of the match counter.

By setting a limit for the period counter, above which no action is taken, a low-pass filter is created allowing lower frequency and harmless triggers to run at full efficiency. Adding a lower period-count value—below which no action is taken—creates a band-pass filter. Setting these maxima and minima allow the system to be tuned to a particular band of trigger frequencies.

4.2.4. Period matching accuracy

To ensure intervals between successive triggers with only a slight mismatch are still detected, the delta-period value of successive triggers was calculated and period-match decided on the size of this number. Increasing this threshold allows a relatively wide range of triggers to be matched. This could be called something like a dynamic-centred band-pass filter.

4.2.5. FFTV operation

The operation of the algorithm in an FPGA is best demonstrated using the output from the ModelSim[5] simulation shown in Figs. 16–18 below. In all cases the system was configured with the values given in Table 6. These values were chosen simply to illustrate the performance of the algorithm and do not represent proposed values for actual ATLAS operation.

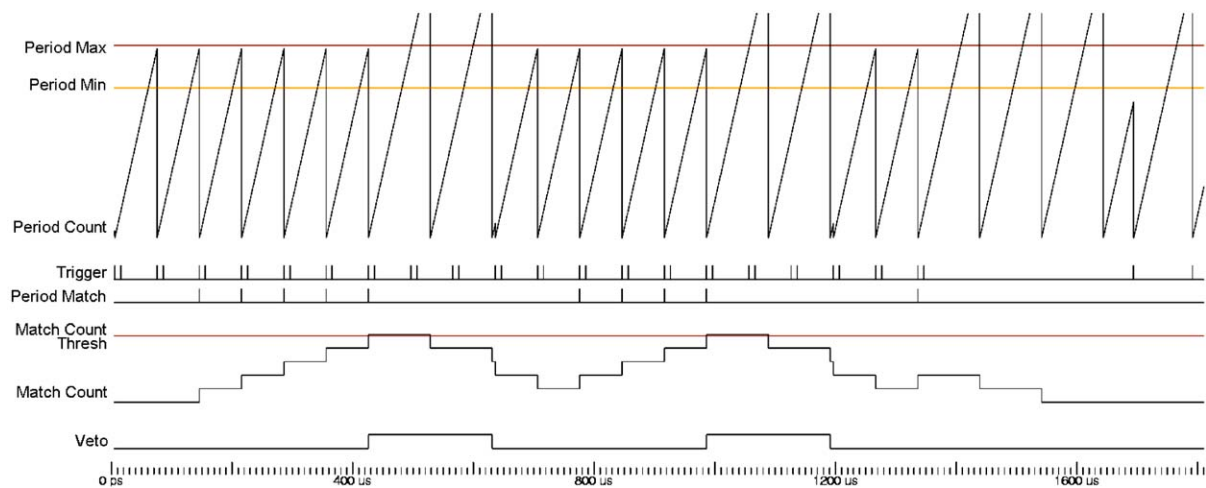[5]Mentor Graphics, http://www.model.com/.

Fig. 17. Demonstrates a pair of repetitive triggers—running at equal rates, but offset—still generating a veto.
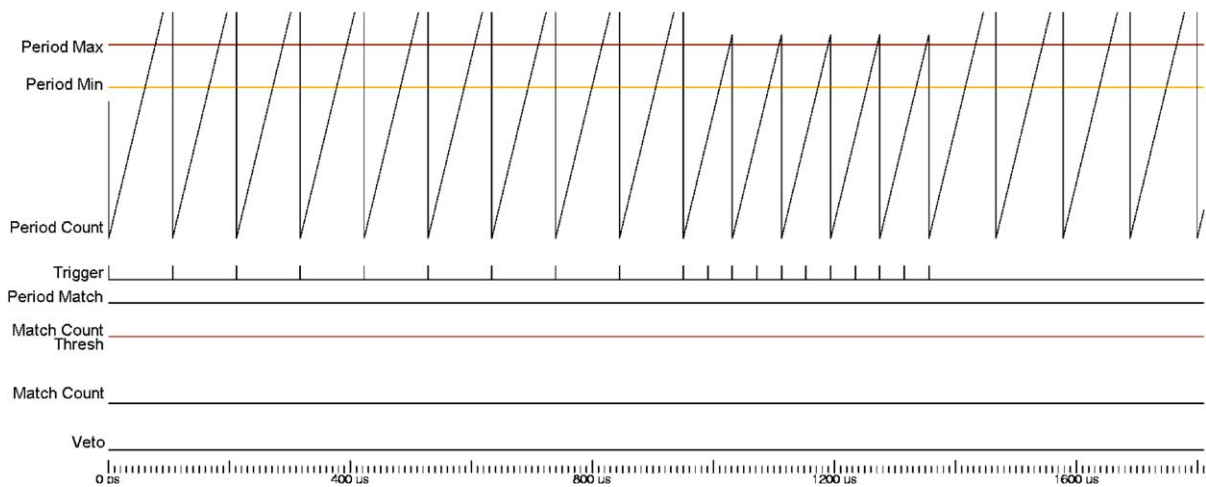

Fig. 18. Demonstrates trigger below and above threshold being ignored. Note that short periods are ignored and used as part of longer period components.

Table 6
Parameter values for the FFTV algorithm in the FPGA

Quantity	Value	Units
Period upper limit	2850	Clock cycles (25 ns)
Period lower limit	2200	Clock cycles (25 ns)
Period roll-over	4100	Clock cycles (25 ns)
Delta-period	127	Clock cycles (25 ns)
Period math threshold	5	—
Veto duration	8000	Clock cycles (25 ns)

4.2.6. Fitting into hardware

The system as described was built as a user configurable module (either through compile-time constants, or registers accessible to the user). Compiling and fitting it for a Xilinx Spartan II 600E FPGA, as used on the TIM, generated a configuration utilising just 2% of logic resources.

4.2.7. Operation in ATLAS

During ATLAS operation, the FFTV would be used to veto ATLAS L1 triggers by the use of the ROD BUSY signal which instructs the ATLAS Central Trigger Processor not to issue any further L1 triggers, until the signal has been removed. The number of clock cycles during which the veto is on will be monitored by the SCT VME system and an alarm will be raised if the resulting fraction of dead time is above a very low threshold.

5. Conclusions

Resonant bond wire vibrations were studied by imaging the bond wire with a high-magnification CCD camera. A novel way of detecting resonant bond wire vibrations in a magnetic field was developed based on measuring the back e.m.f. The two methods gave consistent results but the back emf method was sensitive to lower amplitude vibrations.

Resonant bond wire vibrations will occur if there is a time varying current perpendicular to a magnetic field. If the bond wires are longer than about 2 mm and the magnetic field is in the plane of the loop of the bond wire, currents of a few mA with a frequency close to the resonant frequency of the wire bond will lead to large amplitude vibrations. These large amplitude vibrations are very dangerous and will typically cause the wire bond to fail after a few minutes of operation. The problem turns out to be less severe in the ATLAS SCT because of a combination of the favourable orientation of the wire bonds with the magnetic field (barrel opto-package) and very short wire bonds (forward). A large additional safety factor can be obtained by vetoing fixed frequency running. A suitable algorithm has been developed and will be implemented in ATLAS.

References

[1] G. Bolla, et al., Nucl. Instr. and Meth. A 518 (2004) 277.
[2] J. Goldstein, private communication.
[3] ATLAS Inner Detector Technical Design Report, CERN/LHCC/97-16/17.
[4] ATLAS Pixel Detector Technical Design Report, CERN/LHCC/98-13.
[5] D.G. Charlton, et al., Nucl. Instr. and Meth. A 443 (2000) 430.
[6] Eric Weisstein's World of Physics, http://scienceworld.wolfram.com/physics/beam.html.
[7] See www.autofea.com for program details.
[8] D.J. White, et al., Nucl. Instr. and Meth. A 457 (2001) 369.
[9] P.K. Teng, et al., Nucl. Instr. and Meth. A 497 (2003) 294.
[10] M.-L. Chu, The SCT Barrel Opto-package, EDMS note ATL-IS-AT-0009, available from https://edms.cern.ch/cedar/plsql/edmsatlas.home.
[11] M.-L Chu, The SCT End Cap Opto-package, EDMS note ATL-IS-ES-0094, available from https://edms.cern.ch/cedar/plsql/edmsatlas.home.
[12] L. Feld, SCT End Cap K5 hybrid, EDMS note ATL-IS-EN-0009, available from https://edms.cern.ch/cedar/plsql/edmsatlas.home.
[13] J. Butterworth, et al., TIM (TTC interface module) for ATLAS SCT & pixel read out electronics, Seventh Workshop on LHC Electronics, Stockholm, October 2001, CERN/LHCC/2001/-034.
[14] J. Goldstein, private communication.
[15] N. Ellis, private communication.